RSC Advances

PAPER

View Article Online
View Journal | View Issue

Cite this: *RSC Adv.*, 2015, **5**, 5591

Investigation of luminescence properties and the energy transfer mechanism of $Li_6Lu(BO_3)_3:Ce^{3+}$, Tb^{3+} green-emitting phosphors

Irish Valerie B. Maggay, Pin-Chun Lin and Wei-Ren Liu*

Received 16th October 2014
Accepted 11th December 2014

DOI: 10.1039/c4ra12538j

www.rsc.org/advances

$Li_6Lu(BO_3)_3:Ce^{3+}$, Tb^{3+} phosphor was synthesized *via* a conventional solid-state method. The phase purity, photoluminescence properties, energy transfer mechanism, thermal stability and chromaticity coordinates were investigated. The absorption spectrum was comprised of broad bands in the UV region and the emission spectrum was consisted of characteristic peaks from both Ce^{3+} and Tb^{3+} under UV excitation. The amount of Ce^{3+} was fixed to 3 mol% while Tb^{3+} was varied from 20 to 80 mol% and the chromaticity coordinates were tuned from the blue to green region. The energy transfer mechanism between Ce^{3+} and Tb^{3+} was attributed to a quadrupole–quadrupole interaction and the critical distance was measured to be 8.12 Å. The overall performance of the phosphor was enhanced by the efficient energy transfer between Ce^{3+} and Tb^{3+} ions.

Introduction

White light emitting diodes (W-LEDs) have provided remarkable advances in lighting technologies and displays. They have gained significant attention over conventional lighting sources due to their advantages such as low energy consumption, long operational lifetime, high efficiency, high stability and less environmental threat.[1–11] Commercially available W-LEDs are fabricated by combining a blue emitting InGaN-based LED chip covered by a yellow emitting phosphor $Y_3Al_5O_{12}:Ce^{3+}$ (YAG).[1,2,4,6,7,10,11] However, YAG suffers from inevitable drawbacks such as low color rendering index (CRI) (Ra < 80) and high correlated color temperature (CCT) (T_c > 4500 K) due to the insufficient red emission in the visible spectrum.[1–4,6–8,10,11] Moreover, blue LED chip and yellow phosphor have different degradation rates causing chromatic aberration and decreased efficiency over long period of time.[1] To overcome these defects, a new method has been developed by coupling red, green and blue tricolor phosphors with n-UV LED chip in order to produce high CRI, high color stability and good color uniformity.[1,2,6,7,10] Thus, developments of new phosphors with high chemical stability and strong absorption in UV or near-UV region with high conversion efficiency are highly crucial.[1–3,10]

Borate compounds are widely used in nonlinear optics, piezo and scintillation techniques and phosphors for W-LEDs[12] due to its low synthesizing temperature and high physical and chemical stability.[2] Recent investigations were conducted on $NaSrBO_3:Ce^{3+}$,[2] $MSr_4(BO_3)_3:Ce^{3+}$ (M = Li and Na),[3] $Ca_3Y_2(BO_3)_4:Eu^{3+}$,[4] $Na_3La_2(BO_3)_3:Ce^{3+}$, Tb^{3+},[5] $KSr_4(BO_3)_3:Eu^{3+}$,[7] $LiSr_4(BO_3)_3:Ce^{3+}$, Eu^{2+},[11] $LiCaBO_3$,[13] $Ba_2Ca(BO_3)_2:Ce^{3+}$ [14] and $KCa_4(BO_3)_3:Ln^{3+}$ (Ln = Dy, Eu, Tb).[15] ($Li_6Ln(BO_3)_3$ (Ln = Gd, Y) were investigated and showed promising results on W-LEDs and nonlinear optics application.[12,17–19] $Li_6Lu(BO_3)_3$ host was first synthesized and studied by Yang *et al.*[16] and Fawad *et al.*[20] and it exhibited potential applications for neutron detection scintillator).

Energy transfer plays a crucial role in enhancing the luminescent properties of rare earth ions such as Tb^{3+} and Eu^{3+} which display only narrow excitation peaks near UV region due to the forbidden f–f transition and only yield sharp and weak emission peaks.[1] Ce^{3+} is not only used as an activator but also as a sensitizer. It can generate strong excitation peaks near UV region and can provide efficient conversion to longer wavelengths.[22] Several Ce^{3+} and Tb^{3+} co-doped phosphors were synthesized such as $Ba_3Gd(PO_4)_3:Ce^{3+}$, Tb^{3+},[1] $Na_3La_2(BO_3)_3:Ce^{3+}$, Tb^{3+},[5] $SrMgSi_2O_6$:Ce, Tb,[6] $Sr_2B_5O_9Cl:Ce^{3+}$, Tb^{3+},[8] $BaAl_2B_2O_7:Ce^{3+}$, Tb^{3+},[9] $Sr_3MgSi_2O_8:Ce^{3+}$, Tb^{3+},[10] $SrAl_2B_2O_7:Ce^{3+}$, Tb^{3+},[21] $Ca_3Y_2Si_3O_{12}:Ce^{3+}$, Tb^{3+} [23] and so on.

To the best of our knowledge, the luminescence properties of $Li_6Lu(BO_3)_3:Ce^{3+}$, Tb^{3+} have not been investigated yet. Borate host phosphors have lower synthesizing temperature than that of other host phosphors, such as silicon-based, aluminum-based and nitride-based system. These borate-based phosphors, such as $Sr_2B_2O_5:Ce^{3+}$, Tb^{3+} (1073 K), $NaCaBO_3$ (1123 K), $KCa_4(BO_3)_3$ (1073 K) have been reported.[2,15,26,27] In this study, pure phased-$Li_6Lu(BO_3)_3$ was obtained at a much lower temperature of 973 K with high purity, providing an energy-saving and cost effective advantages over other phosphors. In this study, the crystal structure, photoluminescence (PL) properties, color chromaticity,

Chung Yuan Christian University, Department of Chemical Engineering, Chung Li, Taiwan. E-mail: WRLiu1203@gmail.com

energy transfer mechanism between the sensitizer and activator, and thermal quenching were investigated. The results indicate that $Li_6Lu(BO_3)_3$:Ce^{3+}, Tb^{3+} is a potential green emitting phosphor for UV-LED applications.

Experimental section

Materials and synthesis

A series of rare earth-doped $Li_6Lu(BO_3)_3$:xCe^{3+}, yTb^{3+} ($x = 0.005$, 0.01, 0.03, 0.05, 0.07, 0.10 mol and $y = 0.20$, 0.40, 0.60, 0.70 and 0.80 mol) phosphors were synthesized *via* solid state reactions. The reactants used were Li_2CO_3 (99.99%, Aldrich), H_3BO_3 (99.99%, Aldrich), Lu_2O_3 (99.99, Aldrich), CeO_2 (99.99%, Aldrich) and Tb_4O_7 (99.99%, Aldrich). The stoichiometric proportions of the precursors were weighed and thoroughly ground in an agate mortar. Subsequently, the powder was heated at 973 K for 8 hours under a reducing atmosphere (15% H_2/85% N_2). The products were then cooled down to ambient temperature and ground for further analyses.

Materials characterization

The crystallinity of the as-synthesized samples were characterized using X-ray diffractometer with Cu Kα (λ = 1.5418 Å) generated at 45 kV and 30 mA. Data were gathered in the 2θ range of 10° to 80° with a scan speed of 5° min^{-1}. The luminescence properties of the samples were determined using PL/PLE at room temperature and were recorded by a Spex-Fluorolog-3 spectrophotometer equipped with 450 W Xenon light source and measured with a scan rate of 150 nm min^{-1}. Commission International de I'Eclairage (CIE) chromaticity coordinates of the samples were measured using a Laiko DT-101 color analyzer equipped with a CCD detector (Laiko Co., Tokyo, Japan).

Results and discussion

XRD and crystal structure investigation

The X-ray powder diffraction (XRD) patterns of $Li_6Lu(BO_3)_3$ doped with $0.03Ce^{3+}$, $0.80Tb^{3+}$ and $0.03Ce^{3+}$, $0.65Tb^{3+}$ are presented in Fig. 1. The data indicate that the peaks of the samples were consistent with the standard JCPDS #83-0843 and no impurities were observed even with heavy doping of Tb^{3+} ions. Therefore, pure-phased samples were obtained. Lu^{3+} ions were successfully substituted by Ce^{3+} ions and Tb^{3+} ions due to their comparable ionic radii (Lu^{3+} = 0.977 Å, Ce^{3+} = 1.14 Å, Tb^{3+} = 1.04 Å). $Li_6Lu(BO_3)_3$ host phosphor belongs to the monoclinic system of $Li_6RE(BO_3)_3$ (RE = Gd, Y, Yb, Ho) and space group of $P2_1/c$.[12,16,17] The lattice parameters were calculated to be a = 0.7236 nm, b = 1.6584 nm, c = 0.6693 nm and β = 105.42°. The crystal structure of $Li_6Lu(BO_3)_3$ is shown in Fig. 2(a). The structural unit of $Li_6Ln(BO_3)_3$ (Ln = Gd, Y, Lu) consists of isolated boron with a triangular coordination with oxygen atoms, Li^+ ions surrounded by four or five oxygen atoms forming trigonal bipyramids or tetrahedron prisms, and distorted eight-fold Lu^{3+} with C_1 site symmetry. LuO_8 polyhedra are connected

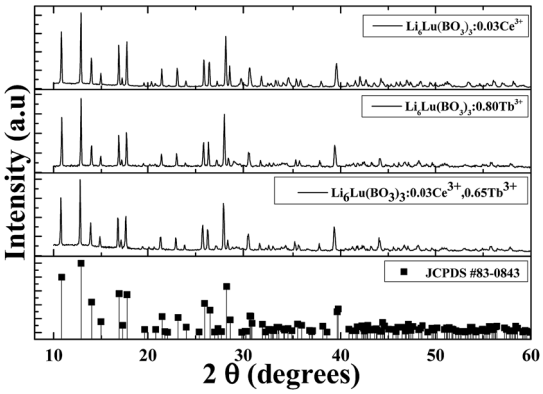

Fig. 1 XRD patterns of different samples synthesized at 973 K for 8 hours under 15% H_2/85% N_2 reducing atmosphere.

with each other by common edges along the direction oblique to the c axis.[9,12,18]

Photoluminescence properties of $Li_6Lu(BO_3)_3$:xCe^{3+}

Fig. 3 illustrates the PL/PLE of $Li_6Lu(BO_3)_3$:xCe^{3+}. When the sample is excited at 350 nm it displays an asymmetric broad band from 360–480 nm. This phenomenon was due to the dual emission of Ce^{3+} attributed to the parity allowed transition from the lowest 5d level to the $^2F_{5/2}$ and $^2F_{7/2}$ ascribed to the spin–orbit coupling of the 4f ground state of Ce^{3+}.[6,9,10,23] The emission band can be decomposed into two Gaussian profiles with maximum peaks at approximately 382 nm (26 178 cm^{-1}) and 415 nm (24 096 cm^{-1}) depicted in the inset with a difference of approximately 2082 cm^{-1}. This result is comparable to the theoretical value of ≈2000 cm^{-1}.[2,10,11] The excitation spectrum monitored at 400 nm consists of two broad bands with maximum peak at 350 nm which was due to the 4f → 5d transition of Ce^{3+}.[1,2,6,8,9,21]

A series of 0.005, 0.01, 0.03, 0.05, 0.07 and 0.10 mol concentration of Ce^{3+} were prepared and is presented in Fig. 4. It is evident that the emission intensity of samples initially increased as Ce^{3+} concentration increased until it reached maximum intensity at 3 mol%. Further increase of Ce^{3+} concentration resulted in decreased intensity due to the concentration quenching of the Ce^{3+}. Also, it is noticeable

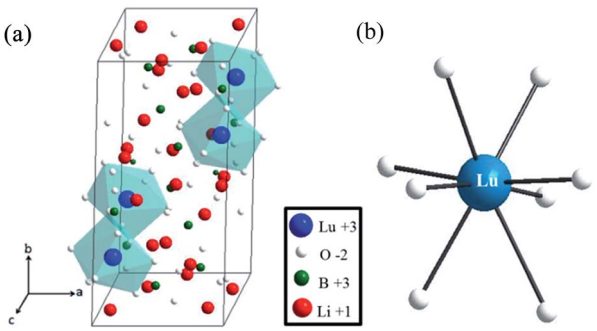

Fig. 2 (a) Crystal structure of $Li_6Lu(BO_3)_3$ and (b) coordination environment of Lu^{3+} ion.

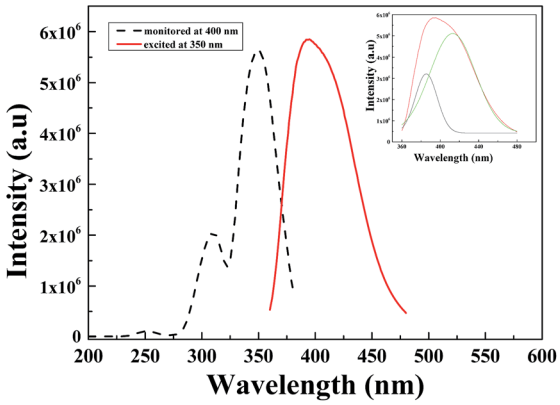

Fig. 3 PL/PLE of $Li_6Lu_{0.97}(BO_3)_3$:0.03Ce^{3+} excited at 350 nm and monitored at 400 nm. Inset shows the Gaussian deconvolution of Ce^{3+} emission.

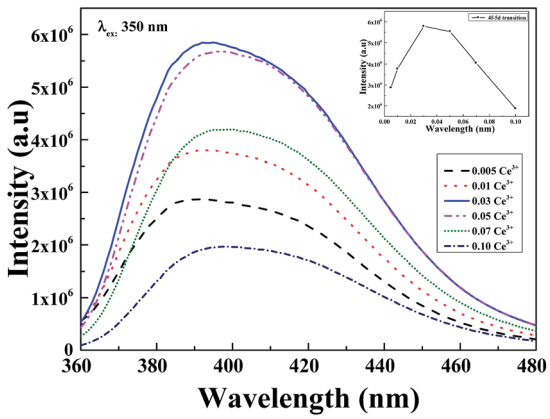

Fig. 4 PL of $Li_6Lu_{1-x}(BO_3)_3$:xCe^{3+} (x = 0.5, 1, 3, 5, 7 and 10 mol%) excited at 350 nm. Inset: PL intensity of $Li_6Lu(BO_3)_3$:Ce^{3+} as a function of Ce^{3+} concentration.

that the emission spectra are shifted to a longer wavelength at higher Ce^{3+} concentration and the peak emission is red shifted from 388 nm to 398 nm which is attributed to the increase of crystal field effect.[8]

Photoluminescence properties of $Li_6Lu_{1-y}(BO_3)_3$:yTb^{3+}

The ground state for Tb^{3+} ions with $4f^8$ configuration is ^7F_J. When Tb^{3+} is excited it is promoted to the 5d shell which generates two $4f^75d^1$ excitation states, a high spin state with ^9D_J configurations or a low spin state with ^7D_J configurations. According to Hund's rule, ^9D_J levels have lower energy; as a result the transitions from $^7F_J \rightarrow {}^9D_J$ are spin–forbidden while $^7F_J \rightarrow {}^7D_J$ transitions are spin-allowed.[23] Fig. 5 shows the PL/PLE of $Li_6Lu_{1-y}(BO_3)_3$:yTb^{3+}. The absorption spectrum monitored at 543 nm is comprised of narrow peaks from 200–275 nm attributed to the spin allowed $4f^8 \rightarrow 4f^75d^1$ transition and sharp peaks from 300–400 nm located at 281, 303, 319, 342, 354, 360 and 377 nm due to the forbidden 4f–4f transitions of Tb^{3+} ions from $^7F_6$, to ^5I_J, ^5H_J, $^5D_{0,1}$, $^5G_{2,3,4}$, $^5D_2$, $^5L_{10}$, and $^5D_3$ levels, respectively.[8] The highest peak is centered at

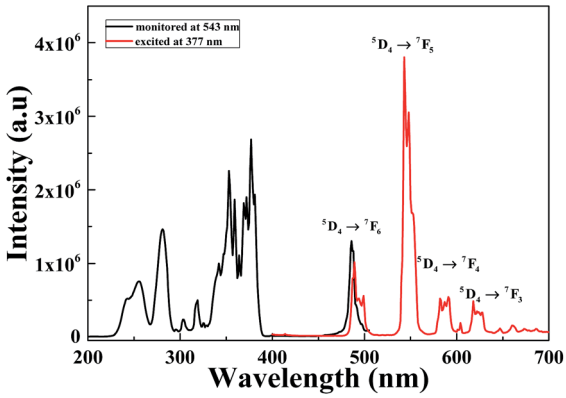

Fig. 5 PL/PLE of $Li_6Lu_{0.40}(BO_3)_3$:0.60Tb^{3+} excited at 377 nm and monitored at 543 nm.

377 nm indicating that the phosphor can be efficiently excited by n-UV chips. Tb^{3+} can be an activator for blue and green phosphors. At lower concentration, it emits blue color on the other hand, at higher concentrations, it exhibits green emission. When the sample is excited at 377 nm, the emission spectrum exhibits four sharp peaks located at 489 nm, 543 nm, 591 nm and 618 nm which are assigned to the $^5D_4 \rightarrow {}^7F_J$ (J = 6, 5, 4 and 3) ascribed to the characteristic transition of Tb^{3+}, respectively. The phosphor exhibits green emitting hue due to the maximum peak at 543 nm corresponding to $^5D_4 \rightarrow {}^7F_5$ transition that is due to magnetic dipole transition.

Different concentrations of $Li_6Lu_{1-y}(BO_3)_3$:yTb^{3+} (y = 0.20–0.80 mol) were synthesized and its corresponding emission intensities are illustrated in Fig. 6. The luminescence intensity of samples increased gradually as the concentration of Tb^{3+} ions increased. It reached maximum intensity at 60 mol% and began to decrease. This phenomenon is a result of the concentration quenching of the Tb^{3+} ions. $^5D_3 \rightarrow {}^5D_4$ is resonant with $^7F_6 \rightarrow {}^7F_0$ transition therefore, the emission due to $^5D_3 \rightarrow {}^7F_J$ transitions are often quenched at high Tb^{3+} content because of the cross relaxation $^5D_3 + {}^7F_6 \rightarrow {}^5D_4 + {}^7F_0$.[1,9] The concentration

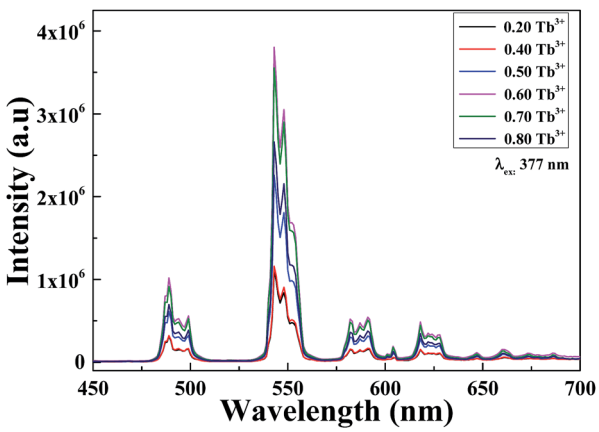

Fig. 6 PL of $Li_6Lu_{1-y}(BO_3)_3$:yTb^{3+} (y = 20, 40, 50, 60, 70, and 80 mol%) excited at 377 nm.

quenching is higher than most Tb^{3+} doped phosphors. A possible reason is linked to the structure of $Li_6Lu(BO_3)_3$ which the zigzag structure of the activator ion restrict the energy migration to one dimension. Therefore, the probability of the migrating excitation to encounter the randomly distributed killer site is lessened.[10,12,17]

Photoluminescence properties of $Li_6Lu_{0.97-y}(BO_3)_3$:0.03Ce^{3+}, yTb^{3+}

The 5d–4f transition of Ce^{3+} is electric dipole allowed and is evidently stronger compared to the 4f–4f intra-configurational transition of Tb^{3+}. Fig. 7(a)–(c) depict the PL/PLE comparison of singly doped Ce^{3+}, Tb^{3+} and Ce^{3+}–Tb^{3+} co-doped $Li_6Lu(BO_3)_3$ phosphor. It is evident that there is a spectral overlap between the emission spectrum of Ce^{3+} in Fig. 7(a) and excitation spectrum of Tb^{3+} in Fig. 7(b) which implies that energy transfer between Ce^{3+} and Tb^{3+} is expected in $Li_6Lu(BO_3)_3$ host. In Fig. 7(c), there is an obvious overlap between the emission and excitation spectra of Ce^{3+}–Tb^{3+} co-doping that verifies that the energy absorbed by Ce^{3+} is efficiently transferred to Tb^{3+} thus, Ce^{3+} is an efficient sensitizer for Tb^{3+}. Furthermore, there is a broad absorption band at UV region attributed to Ce^{3+} which makes it suitable to be excited by n-UV LED chip.

Energy transfer between sensitizer and activator enhances the emission intensity. Fig. 8 illustrates the investigation of series of phosphors co-doped with 3 mol% of Ce^{3+} and varying concentrations of Tb^{3+} (y = 20–80 mol%) excited at 350 nm. The broad band situated from 360–450 nm is ascribed to the 5d–4f transition of Ce^{3+} ions while the narrow peaks 475–650 nm are assigned to the $^5D_4 \rightarrow {}^7F_J$ (J = 6, 5, 4 and 3) transitions of Tb^{3+} with maximum peak at 543 nm emitting a green color. The PL intensity initially increased as the concentration of Tb^{3+} increased until it reached its optimum concentration at x = 0.03, y = 0.65. As the Tb^{3+} concentration further increased, the emission intensity decreased as a result of concentration quenching. Conversely, the intensity of Ce^{3+} is inversely proportional to the concentration of Tb^{3+}. These results denote that an effective energy transfer occurred. Moreover, comparing the PL of Fig. 8 with Fig. 6, it is highly evident that the intensity of Ce^{3+}–Tb^{3+} co-doping is higher than singly doped Tb^{3+} proving that Ce^{3+} is an efficient sensitizer.

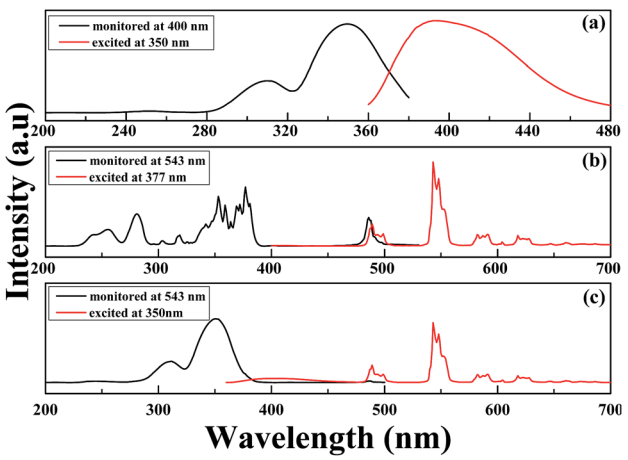

Fig. 7 (a). PL/PLE of $Li_6Lu(BO_3)_3$:0.01Ce^{3+} excited at 350 nm and monitored at 400 nm; (b) PL/PLE of $Li_6Lu(BO_3)_3$:0.60Tb^{3+} excited at 377 nm and monitored at 543 nm; (c) PL/PLE of $Li_6Lu(BO_3)_3$:0.03-Ce^{3+},0.65Tb^{3+} excited at 350 nm and monitored at 543 nm.

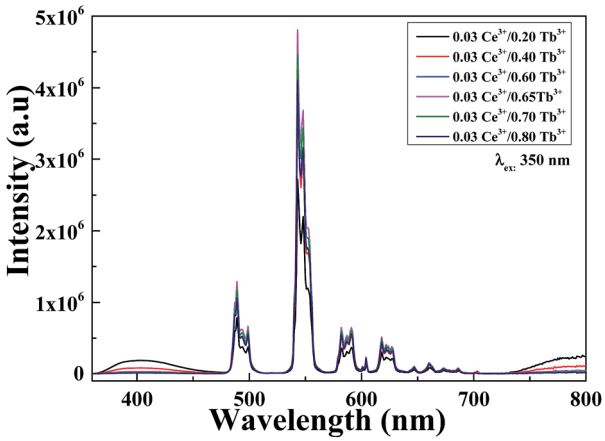

Fig. 8 PL of $Li_6Lu(BO_3)_3$:0.03Ce^{3+}, yTb^{3+} (y = 20, 40, 60, 65, 70 and 80 mol%) excited at 350 nm and monitored at 543 nm.

Schematic diagram of energy transfer

The energy levels and energy transfer mechanism are illustrated in the schematic diagram in Fig. 9. When excited at 350 nm, Ce^{3+} ions are excited to the 5d configuration then the ions relax non-radiatively to the lowest of 5d state. The excited ions return to its ground state at $^2F_{5/2}$ and $^2F_{7/2}$ levels with a consequent broad band emission. As a consequence of the matched energy levels of Ce^{3+} and Tb^{3+}, the sensitizer (Ce^{3+}) can transfer its energy to the activator (Tb^{3+}) thence causing Tb^{3+} ions to excite from its ground state. Tb^{3+} ions relax at level $^5D_3$ with subsequent $^5D_3 \rightarrow {}^7F_J$ transitions. Cross-relaxation might occur between $^5D_3$ and $^5D_4$ simultaneously with increasing amount of Tb^{3+} generating stronger emissions and higher intensities at $^5D_4 \rightarrow {}^7F_J$ transitions while leading to a decrease in $^5D_3$ emission. Finally, the excited Tb^{3+} ions return

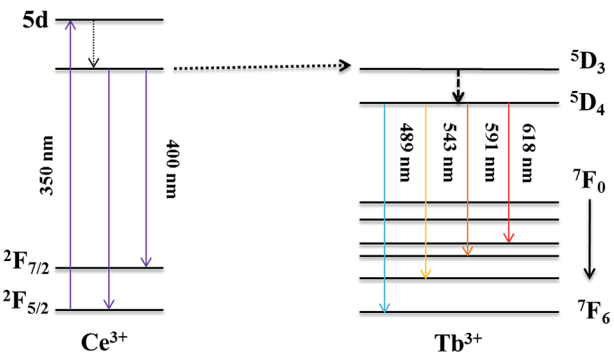

Fig. 9 The schematic energy levels of Ce^{3+} and Tb^{3+} with energy transfer mechanism.

to its ground state with a subsequent emission of green luminescence.[1,6]

$Ce^{3+} \rightarrow Tb^{3+}$ energy transfer

In order to further analyze the energy transfer between Ce^{3+} and Tb^{3+}, Fig. 10 presents the energy transfer efficiency of Ce^{3+} and Tb^{3+}, 4f–5d transition of Ce^{3+} and $^5D_4 \rightarrow {}^7F_5$ transition of Tb^{3+} all as a function of Tb^{3+} concentration in $Li_6Lu(BO_3)_3$ phosphor excited at 350 nm. The energy transfer efficiency (η_{ET}) can be calculated using following equation:[1,6,8,9]

$$\eta_{ET} = 1 - \frac{I_S}{I_{S0}} \quad (1)$$

where I_S and I_{S0} are the luminescence intensities of Ce^{3+} in the presence and absence of Tb^{3+}, respectively. The value of η_{ET} increased gradually with an increase of Tb^{3+} concentration. When Tb^{3+} concentration increased to 65 mol%, the η_{ET} increased to 99.60% indicating efficient energy transfer between the sensitizer and activator. The intensities of 4f–5d transition of Ce^{3+} decreased as the amount of Tb^{3+} increased thus the energy of Ce^{3+} ions is successfully transferred to its neighboring Tb^{3+} ions. On the other hand, Tb^{3+} initially increased until it decreased an optimum concentration at 65 mol% and eventually decreased with further addition of Tb^{3+} into the host.

Besides from spectral overlap, efficient energy transfer involves strong interactions. It may transpire under radiative transfer through photons which is nearly distance independent and non-radiative transfer which is associated with the resonance between the donor and acceptor. It can be either exchange interaction or multipolar interaction.[24,25] To calculate the critical distance (R_c) between Ce^{3+} ions and Tb^{3+} ions, the following equation is used:[9,10,24]

$$R_c \approx 2\left[\frac{3V}{4\pi\chi_c N}\right]^{1/3} \quad (2)$$

where V is the volume of the unit cell ($V = 762.43$ Å^3), χ_c is the total concentration of Ce^{3+} and Tb^{3+} at maximum intensity ($\chi_c = 0.68$) and N is the number of host cations in the unit cell ($N = 4$).

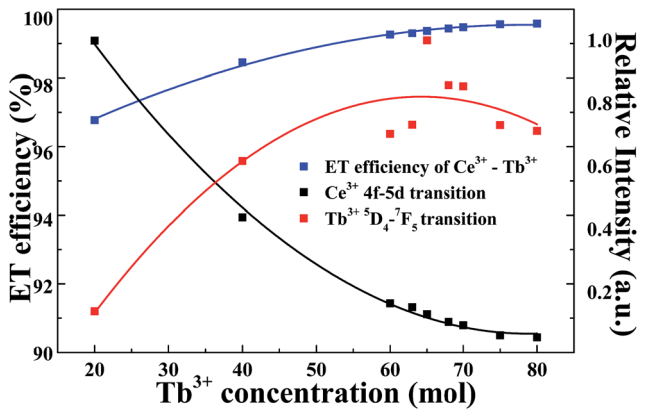

Fig. 10 Dependence of Ce^{3+} emission (4f → 5d), Tb^{3+} emission ($^5D_4 \rightarrow {}^7F_5$) and energy transfer efficiency as a function of Tb^{3+}.

Using eqn (2) the calculated critical distance is approximately 8.12 Å. R_c should be less than 5 Å in an exchange interaction. Thus, the principle governing the energy transfer is multipolar interaction.[5,24] According to Dexter's energy transfer formula of multipolar interaction and Reisfeld's approximation, the following relationship is obtained:[1,6,8,9,24]

$$\frac{\eta_0}{\eta} \propto C_{Ce+Tb}{}^{n/3} \quad (3)$$

where η and η_0 are the luminescence quantum efficiencies of Ce^{3+} with and without Tb^{3+} ions present, respectively. The ratio η/η_0 can be estimated by the ratio of relative emission intensities, I_{S0}/I_S in the absence and presence of activator. C_{Ce+Tb} is the total concentration of Ce^{3+} and Tb^{3+} and $n = 6$, 8 and 10 corresponds to dipole–dipole, dipole–quadrupole and quadrupole–quadrupole mechanisms, respectively.[1,6,8,9,24]

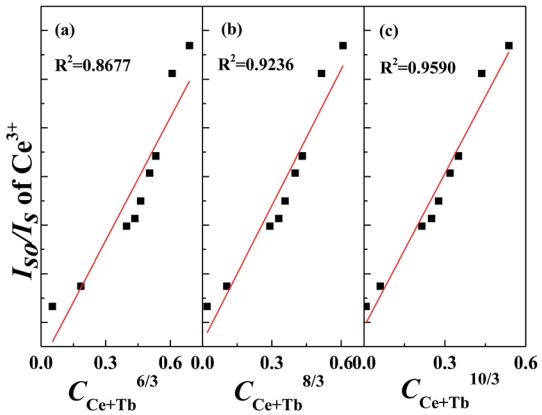

Fig. 11 The dependence of I_{S0}/I_S of Ce^{3+} on (a) $C_{Ce-Tb}{}^{6/3}$, (b) $C_{Ce-Tb}{}^{8/3}$ and (c) $C_{Ce-Tb}{}^{10/3}$.

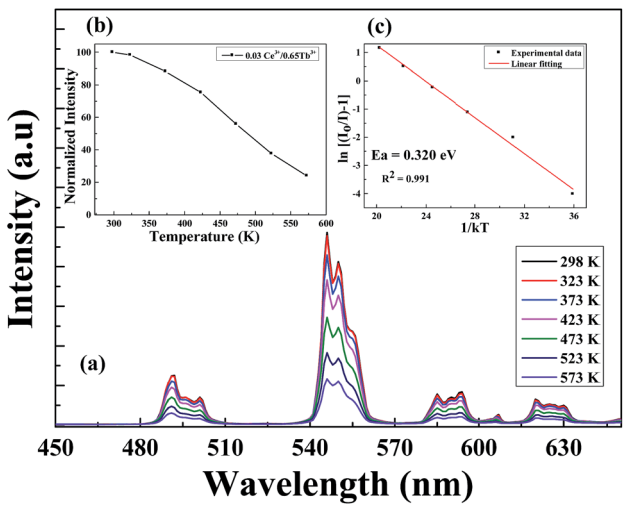

Fig. 12 (a) Thermal luminescence of $Li_6Lu_{0.32}(BO_3)_3$:0.03Ce^{3+}, 0.65Tb^{3+} excited at 350 nm. The insets shows the (b) normalized intensity as a function of temperature and (c) the graph of $\ln[(I_0/I) - 1]$ *versus* $1/\kappa T$.

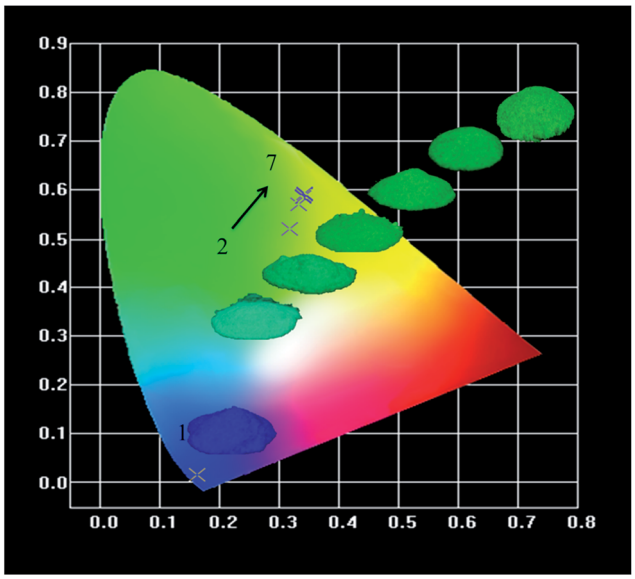

Fig. 13 CIE coordinates of $Li_6Lu_{0.97}(BO_3)_3$:0.03Ce^{3+} and $Li_6Lu_{0.97-y}(BO_3)_3$:0.03Ce^{3+}, yTb^{3+} (y = 0.20 to 0.75) phosphors under 350 nm excitation.

In order to further comprehend the energy transfer mechanism between Ce^{3+} and Tb^{3+} ions, Fig. 11(a)–(c) illustrate the relationships of I_{S0}/I_S and $C^{n/3}$. Among these three, Fig. 10(c) demonstrates the most commendable linear relationship. Therefore, it signifies that the energy transfer mechanism between Ce^{3+} and Tb^{3+} in $Li_6Lu(BO_3)_3$ host is governed by quadrupole–quadrupole interaction.

Aside from high luminescence, another crucial property of LED phosphors is thermal stability predominantly for high power LEDs in which the operating temperature can reach up to 450 K.[12] Fig. 12(a) depicts the temperature dependence of the luminescence intensity of $Li_6Lu(BO_3)_3$:0.03Ce^{3+}, 0.65Tb^{3+} excited at 350 nm in the temperature range of 298 K to 573 K. The maximum peak is constantly located at 543 nm even at higher temperature. The emission intensity progressively decreased as the temperature increased due to thermal quenching. Fig. 12(b) presents the normalized intensity of the thermal luminescence. At 373 K, the thermal luminescence is reduced by almost 12%, at 473 K the intensity is decreased to 50% and at 573 K, the thermal luminescence is reduced by approximately 76%.

To promote better understanding of the relationship between the temperature and luminescence intensity and to determine the activation energy for thermal quenching, the gathered data were fitted to the Arrhenius equation:[12,14]

$$I(T) = \frac{I_0}{1 + A\exp(-\Delta E/\kappa T)} \quad (4)$$

where $I(T)$ is the intensity at given temperature T, I_0 is the initial intensity, A is a constant, κ is the Boltzmann constant (8.617×10^{-5} eV K^{-1}) and E is the activation energy for thermal quenching. Fig. 12(c) plots the $\ln[(I_0/I) - 1]$ *versus* $1/\kappa T$ and the activation energy is calculated to be 0.320 eV. The high activation energy indicates good thermal stability.

CIE coordinates of $Li_6Lu_{0.97}(BO_3)_3$:0.03Ce^{3+} and $Li_6Lu_{0.97-y}(BO_3)_3$:0.03Ce^{3+}, yTb^{3+} phosphors

Commission International de l'Eclairage (CIE) chromaticity coordinates of the samples are presented in Fig. 13 and summarized in Table 1. The CIE coordinates illustrate that with increasing Tb^{3+} concentration, the chromaticity is tuned from blue to green as a result of the cross-relaxation between $^5D_3$ level and $^5D_4$ level. Table 1 also shows the relative intensity of $^5D_4 \rightarrow {}^7F_5$ transition and it indicates that the influence of energy transfer between Ce^{3+} and Tb^{3+} has significantly improved the luminescence properties of the phosphor. At 350 nm, the relative intensity of $Li_6Lu(BO_3)_3$:0.03Ce^{3+}, 0.65Tb^{3+} was enhanced by 178%. It is also noticeable that $Li_6Lu_{0.97}(BO_3)_3$:0.03Ce^{3+} has high color purity.

Conclusions

A series of tunable blue to green emitting $Li_6Lu_{0.97-y}(BO_3)_3$:0.03Ce^{3+}, yTb^{3+} phosphors were successfully synthesized *via* conventional solid state reaction. Pure phased samples were successfully obtained even at high Tb^{3+} doping concentration. The energy absorbed by Ce^{3+} ions were efficiently transferred to Tb^{3+} since the 5d energy level of Ce^{3+} ions is close to the $^5D_3$ level of Tb^{3+} ions resulting in improved photoluminescence properties of the phosphors. The gathered results indicate that Ce^{3+} is an efficient sensitizer for Tb^{3+}. The energy transfer is governed by a resonant type quadrupole–quadrupole

Table 1 Chromaticity coordinates of $Li_6Lu_{0.97}(BO_3)_3$:0.03Ce^{3+} and $Li_6Lu_{0.97-y}(BO_3)_3$:0.03Ce^{3+}, yTb^{3+} phosphors

Phosphors	Excitation wavelength (nm)	CIE chromaticity coordinates		$^5D_4 \rightarrow {}^7F_5$ Relative intensity
		x	y	
1. $Li_6Lu_{0.97}(BO_3)_3$:$_{0.03}Ce^{3+}$	350	0.162	0.015	0
2. $Li_6Lu_{0.77}(BO_3)_3$:$_{0.03}Ce^{3+}$,$_{0.20}Tb^{3+}$	350	0.317	0.519	1.00
3. $Li_6Lu_{0.57}(BO_3)_3$:$_{0.03}Ce^{3+}$,$_{0.40}Tb^{3+}$	350	0.334	0.570	1.43
4. $Li_6Lu_{0.37}(BO_3)_3$:$_{0.03}Ce^{3+}$,$_{0.60}Tb^{3+}$	350	0.340	0.586	1.50
5. $Li_6Lu_{0.32}(BO_3)_3$:$_{0.03}Ce^{3+}$,$_{0.65}Tb^{3+}$	350	0.340	0.588	1.78
6. $Li_6Lu_{0.27}(BO_3)_3$:$_{0.03}Ce^{3+}$,$_{0.70}Tb^{3+}$	350	0.342	0.589	1.64
7. $Li_6Lu_{0.22}(BO_3)_3$:$_{0.03}Ce^{3+}$,$_{0.75}Tb^{3+}$	350	0.342	0.593	1.53

interaction and the energy transfer critical distance is calculated to be 8.12 Å. The high activation energy denotes high thermal stability of the phosphor. The color of $Li_6Lu(BO_3)_3:Ce^{3+}$, Tb^{3+} phosphor can be modified from blue to green under UV radiation and shows a great potential for W-LED applications.

Acknowledgements

This research is supported by the National Science Council of Taiwan under contract numbers: 102-2221-E-033-050-MY2 and 102-3011-P-033-003.

Notes and references

1 Y. Jin, Y. Hu, X. Wang, Z. Mu, G. Ju and Z. Yang, *Phys. B*, 2014, **436**, 105–110.
2 W. R. Liu, C. H. Huang, C. P. Wu, Y. C. Chiu, Y. T. Yeh and T. M. Chen, *J. Mater. Chem.*, 2011, **21**, 6869–6874.
3 C. Guo, X. Ding, H. J. Seo, Z. Ren and J. Bai, *J. Alloys Compd.*, 2011, **509**, 4871–4874.
4 P. L. Lin, Z. P. Yang, Z. J. Wang and Q. L. Guo, *Chin. Phys. Lett.*, 2007, **24**, 2977–2979.
5 M. Yang, L. Liu and F. Chen, *Mater. Lett.*, 2012, **88**, 116–118.
6 X. Fu, L. Fang, S. Niu and H. Zhang, *J. Lumin.*, 2013, **142**, 163–166.
7 Y. Zhang, L. Wu, M. Ji, B. Wang, Y. Kong and J. Xu, *Opt. Mater. Express*, 2012, **2**, 92–102.
8 J. Zheng, C. Guo, X. Ding, Z. Ren and J. Bai, *Curr. Appl. Phys.*, 2012, **12**, 643–647.
9 J. Sun, Y. Sun, J. Lai, Z. Xia and H. Du, *J. Lumin.*, 2012, **132**, 3048–3052.
10 H. Yu, W. Zi, S. Lan, S. Gan, H. Zou, X. Xu and G. Hong, *Opt. Laser Technol.*, 2012, **44**, 2306–2311.
11 Q. Wang, D. Deng, Y. Hua, L. Huang, H. Wang, S. Zhao, G. Jia, C. Li and S. Xu, *J. Lumin.*, 2012, **132**, 434–438.
12 F. Zhang, Y. Wang and Y. Tao, *J. Lumin.*, 2013, **136**, 51–56.
13 L. H. Jiang, Y. L. Zhang, C. Y. Li, R. Pang, J. Q. Hao and Q. Su, *J. Lumin.*, 2008, **128**, 1904–1908.
14 H. Lin, H. Liang, Z. Tian, B. Han, J. Wang, Q. Su and G. Zhang, *J. Phys. D: Appl. Phys.*, 2009, **42**, 1–9.
15 A. A. Reddy, S. Das, A. Goel, R. Sen, R. Siegel, L. Mafra, G. V. Prakash and J. M. F. Ferreira, *AIP Adv.*, 2013, **3**, 1–15.
16 F. Yang, S. K. Pan, D. Z. Ding, X. F. Chen, H. Feng and G. H. Ren, *J. Cryst. Growth*, 2010, **312**, 2411–2414.
17 G. Ju, Y. Hu, H. Wu, Z. Yang, C. Fu, Z. Mu and F. Kang, *Opt. Mater.*, 2011, **33**, 1297–1301.
18 F. Zhang, Y. Wang and Y. Tao, *Phys. Procedia*, 2012, **29**, 55–61.
19 H. Nishimura, S. Hosoya, H. Takashima and Y. Kanno, *Jpn. J. Appl. Phys.*, 2006, **45**, 909–911.
20 U. Fawad, M. Oh, H. Park and H. J. Kim, *J. Korean Phys. Soc.*, 2013, **62**, 1102–1107.
21 Y. Yang, A. Bao, H. Lai, Y. Tao and H. Yang, *J. Phys. Chem. Solids*, 2009, **70**, 1317–1321.
22 U. Manik, S. C. Gedam and S. J. Dhoble, *J. Lumin.*, 2013, **136**, 191–195.
23 B. V. Rao, Y. T. Nien, W. S. Hwang and I. G. Chen, *J. Electrochem. Soc.*, 2009, **156**, J338–J341.
24 I. V. B. Maggay, P. C. Lin and W. R. Liu, *J. Solid State Lighting*, 2014, **1**, 1–15.
25 G. Ju, Y. Hu, L. Chen, X. Wang, Z. Mu, H. Wu and F. Kang, *J. Electrochem. Soc.*, 2011, **158**, J294–J299.
26 J. Sun, J. Lai, J. Zhu, Z. Xia and H. Du, *Ceram. Int.*, 2012, **38**, 5341–5345.
27 J. Sun, Z. Lian, G. Shen and D. Shen, *RSC Adv.*, 2013, **40**, 18395–18405.